He-vacancy interactions in Si and their influence on bubble formation and evolution

V. Raineri and S. Coffa
CNR-IMETEM, Stradale Primosole 50, I-95121 Catania, Italy

E. Szilágyi
Research Institute for Particle and Nuclear Physics, P.O. Box 49, H-1525 Budapest, Hungary

J. Gyulai
Research Institute for Technical Physics and Materials Science (MTA-MFA), P.O. Box 49, H-1525 Budapest, Hungary

E. Rimini
INFM and Dipartimento di Fisica, Corso Italia 57, I-95129 Catania, Italy
(Received 23 April 1999; revised manuscript received 21 July 1999)

The mechanisms of He bubble and, after annealing, of void formation have been investigated for single and multiple He^+ implants in Si. Several analytical techniques have been adopted: photoluminescence (PL), Rutherford backscattering of protons, transmission electron microscopy, and atomic force microscopy. When a second implant is performed a systematic enlargement of the bubble band reveals the importance of the interaction between He atoms and point defects generated during irradiation. Size effects of the implanted region protrusions indicated a He diffusion mechanism and an interaction with vacancies and divacancies for the bubble formation. PL spectra indicate the presence of complexes helium divacancies in the same temperature where self-interstitials annihilate at the sample surface. The interaction of helium atoms with divacancies allows the inversion in the vacancy-interstitial balance producing a supersaturation of vacancies in the silicon bulk. This vacancy supersaturation causes the observed annihilation of interstitial type defects after a suitable annealing.

I. INTRODUCTION

Helium is known to agglomerate into bubbles when implanted in metals[1–3] or in semiconductors.[4,5] In the past, due to the technological interest, these studies have been devoted to understand the effects on the first-wall materials in a fusion or fission reactor environment.[6–8]

Recently, the investigation of He-bubble formation in Si and the subsequent transition to voids by thermal annealing has received a lot of interest also in view of possible applications in silicon device fabrication. Voids can be obtained implanting other light species, however, helium presents many advantages: due to its high permeability it evaporates easily from the silicon wafer while, being an inert gas, does not interact with silicon atoms, so that no impurity is left and chemical interactions are avoided.

Voids have been demonstrated to be a powerful defect for gettering transition metals.[9,10] On the void internal surface dangling bonds, strongly interacts with point defects, so that they affect the impurity diffusivity and the secondary defect formation and evolution.[11] Moreover, voids introduce deep levels in the silicon band gap and this property can be used to control the minority carrier lifetime in power devices.[12–15]

He bubble and void formation indeed is a quite complex phenomenon and involves several elementary mechanisms. So far, exploring all the peculiarities of the phenomenon and using several techniques, many experiments have been carried out and interesting data accumulated. Recent results obtained by He implants in Si targets at different temperatures (from 77 to 700 K) have clarified the role and the relative relevance of the main factors involved in the bubble formation, i.e., the radiation damage and the short and long range migration of the He atoms.[16]

The supersaturation of noble gas atoms in the lattice leads to formation of bubbles via an interaction with the radiation damage.[16,17] Helium atoms in silicon do not occupy substitutional sites but if by chance they are located in a vacancy site, they move to interstitial positions to minimize the free energy according to molecular dynamic (MD) calculations.[18] Helium is strongly repelled by monovacancies. The electron density, associated with the reconstructed bonds surrounding the vacancy, results in Pauli repulsion with the helium filled electron shell.[18,19] The most stable configuration corresponds to a helium atom in an interstitial site far away from the vacancy. Helium atoms form instead a stable complex with a divacancy or a vacancy clusters according to photoluminescence measurements and MD calculations.[19] These properties we believe are quite important for bubble formation.

In this work we investigate the role played by vacancies, interstitials and helium atoms during bubble and void formation. In particular, we will follow the evolution of vacancy clusters, induced by irradiation, during subsequent thermal treatments and we will clarify the role of helium atoms to stabilize them and to allow void formation. This evolution is quite peculiar of helium implants and differs substantially from that occurring during the annealing of the usual dopant species. The comparison allowed us to understand the reasons of a different equilibrium final condition for the residual defects. Finally, an explanation of the secondary defect annihilation when voids are formed in silicon is given.

II. EXPERIMENTAL DETAILS

Czochralski grown (100) silicon wafers were implanted with He atoms at energies between 20 and 300 keV and in the 3×10^{16}–$1\times10^{17}\,\mathrm{cm}^{-2}$ dose range. The sample temperature during implantation was maintained at $100\pm2\,^{\circ}\mathrm{C}$ by using a thermocouple in contact with the sample surface and a feedback system. All the implants were performed at a fixed dose rate of 1 μA/cm^2.

The annealings were carried out in the temperature range between 200 and 1200 °C by using a horizontal conventional furnace under a continuous nitrogen flux (2 l/min). The temperature ramp during the heating and cooling stage was 10 °C per minute.

The change in volume, caused by the implants, and the void formation were studied by forming adjacent stripes of implanted and unimplanted regions using a photoresist mask, 1.5 μm thick. The helium ions, at energies lower than 80 keV, are stopped in the mask. The resist etching was performed in plasma to obtain 87°-sidewall mask. Solvents were used for the final resist removal to avoid damaging the silicon surface and the generation of artifacts. Unimplanted samples, used as reference, do not show any step or surface artifact introduced by lithography or sample preparation itself within the sensitivity of atomic force microscopy (AFM). The AFM equipment used was a Digital Instruments Dimension 3100 and measurements were carried out in tapping mode.

The He content was determined by p-BS (proton backscattering spectrometry) using 2040 keV $^1H^+$ beam[20,21] obtained from a 5 MeV van de Graaff accelerator of KFKI Research Institute for Particle and Nuclear Physics. The ion beam was collimated to 0.3×1 mm^2 and a current of about 10 nA, as measured by a transmission Faraday cup, was used.[22] The p-BS experiments were performed at 1×10^{-4} Pa vacuum using a 25 mm^2 ORTEC detector at 165° scattering angle with a solid angle of 2.55 msr. The integrated charge of each measurement was 40 μC. To improve the depth resolution of the measurements, the sample was tilted with an angle of 75°. Spectra were analyzed by the RBX program.[23]

Photoluminescence (PL) measurements were performed by pumping with the 488-nm line of an Ar^+ ion laser. The pump power varied between 0.01 and 200 mW over a circular area with a 1 mm diameter and the laser beam was mechanically chopped at 55 Hz. The luminescence signal was analyzed with a monochromator and detected with a liquid nitrogen cooled Ge detector. Spectra were recorded using a lock-in amplifier with the chopper frequency as a reference. Luminescence lifetime measurements were performed by monitoring the decay of the PL signal at 1.54 μm after pumping to steady state and mechanically switching off the laser beam. The overall time resolution of our system is of 30 μs. Low-temperature measurements were performed by using a closed cycle liquid He cooler system with the samples kept in vacuum.

A Jeol 2010 Fx microscope operating at 160 kV was used to carry out transmission electron microscopy (TEM) in cross section or plan view thinned samples. Standard sample preparation by mechanical thinning and subsequent ion milling was used. Analyses were performed both in the pole configuration, i.e., along the [110] direction, or with two beams, i.e., the transmitted beam and the (220) or (111) spot exited for cross or plan view analyses, respectively.

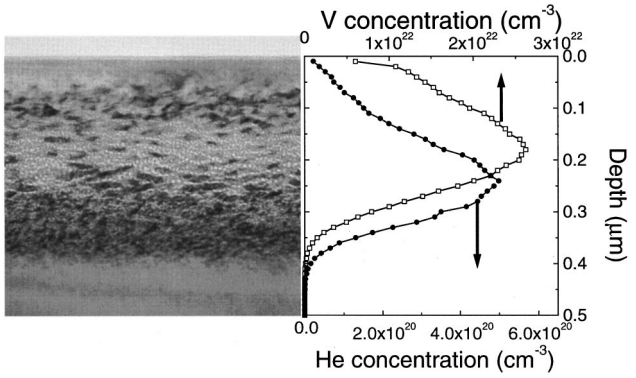

FIG. 1. TEM cross section of an as-implanted sample with 20 keV $1\times10^{17}\,\mathrm{cm}^{-2}$ He ions. The depth profile of He and vacancy distribution as obtained by a SRIM calculation is reported for comparison.

III. SUPERSATURATION OF VACANCIES BY He IMPLANTS

Helium implants in silicon, at fluences higher than $1\times10^{16}\,\mathrm{cm}^{-2}$, induce bubble formation. This critical fluence increases with ion energy because a local helium concentration of $3\times10^{20}\,\mathrm{cm}^{-3}$ should be reached.[13] Bubbles can be observed directly by TEM analyses. As an example, the cross section image of a sample implanted with 20 keV He^+-$1\times10^{17}\,\mathrm{cm}^{-2}$ is reported in Fig. 1. In the same figure the depth profiles of vacancies and He are reported as obtained by SRIM calculations.[24] Bubbles of 4–5 nm in diameter are localized at a depth shallower than the He^+ projected range, in a region where instead the radiation damage peak is located according to SRIM calculations. The bubble band extends between 60 nm and 0.35 μm from the sample surface. In the near surface region (between 120 and 230 nm) a higher density of bubbles is present. This layer is situated where a high vacancy concentration is located according to SRIM. A second layer with a lower bubble concentration extends from 0.23 to 0.35 μm. At deeper depth no bubble is observed. The transition region between the presence and the absence of bubbles is quite sharp and they are accumulated up to this border with no exception. The same characteristics have been observed for implants at energies in the 20–300 keV range.

We have investigated by TEM analyzes the bubble distribution in as-implanted samples when two He implants at different energies were performed in the same samples for several combinations of doses. In the following we describe the results obtained in several experiments performed by implanting sequentially He at different energies. The He bubble region has been observed in the TEM before and after the second implant. The width of the region containing the bubbles formed by the first implant increases in all the investigated cases after the second implant. In particular, bubbles are observed to form at the far-away border of the first and deeper implant even if the energy of the second implant is quite lower than the first one, so that the two He

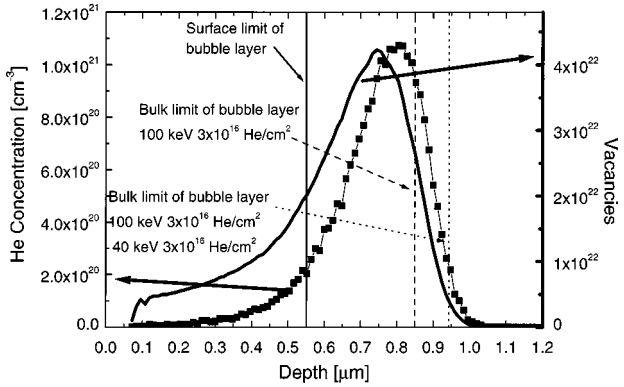

FIG. 2. Depth profile of helium and corresponding vacancy profile as obtained by TRIM calculation for a He ion implantation at 100 keV with a dose of $3\times10^{16}\,\mathrm{cm}^{-2}$. The extension of the bubble layer, obtained by TEM analyses, is also reported for the as-implanted sample (from the continuous vertical line to the vertical dashed line) and after a second implant at 40 keV $3\times10^{16}\,\mathrm{cm}^{-2}$ (from the continuous vertical line to the vertical dotted line).

distributions are well separated. This is a quite surprising result, but it was obtained for several combinations of energies and doses of the two implants. The results of a typical experiment are illustrated in Fig. 2, they refer to a double implant performed in the following sequence 100 keV He^+-$3\times10^{16}\,\mathrm{cm}^{-2}$-40 keV $3\times10^{16}\,\mathrm{cm}^{-2}$. The bubbles after the first 100 keV He^+ implant are located at a depth ranging from 0.55 to 0.85 μm from the surface, respectively. The second implant induces the formation of bubbles deeper up to 0.95 μm, maintaining the near surface depth to 0.55 μm. The full line represents the vacancy concentration as calculated by SRIM after the 100 keV implant, while the dotted line the helium concentration depth profile. This profile is in good agreement with that extracted from p-BS measurements, as shown later.

The borders of the bubble layers determined by the TEM analyses are indicated, for simplicity, as vertical lines. In particular, the near-surface border, that does not change after the second implant, is shown as a continuous line, while the dashed line refers to the deep border after the first implant at 100 keV $3\times10^{16}\,\mathrm{cm}^{-2}$, and the dotted line to the deep border after also the second implant (at 40 keV $3\times10^{16}\,\mathrm{cm}^{-2}$), respectively.

The bubble layer formed during the first He^+ implant is centered round the calculated vacancy distribution. The second implant enlarges the bandwidth, as observed by TEM analyses, toward the bulk. We performed many double implants changing the implant energy sequence but we always observed an enlargement of the preexisting bubble band toward the inside bulk. Moreover, the observed increase in the bandwidth is proportional to the fluence of the second implant. The same enlargement was observed for a second Si self-ion implantation. These results clearly indicate that helium atoms interact with point defects generated during the implant. We believe they are vacancies.

During implant both vacancies and interstitials are formed in the crystal. Soon, they spread in the samples, diffusing to the surface and in the bulk, till they annihilate or they are trapped into more complex defects. The magnitude of the repulsion energy between a monovacancy and a helium atom has been calculated as 1.2 eV, and it is nearly equal to the activation energy for diffusion of isolated helium interstitials (0.84 eV).[19] This fact suggests an unusual mechanism for the enhanced diffusion of the helium impurity: the implant itself causes an above-equilibrium flux of vacancies from the surface into the bulk, the vacancy-He repulsion is large enough to overcome the barrier for diffusion.[19] The helium interstitials are simply pushed and dragged into the bulk by the wave of vacancies coming from the surface. This implies the existence of He atoms inside the as-implanted samples not trapped in bubbles but just dissolved in the matrix in interstitial position. Indeed, their presence in very simple He-V clusters not visible in TEM has already been deduced by He desorption analyses.[25]

Helium atoms instead are stable in a complex with a neutral divacancy.[19] The large drop in energy resulting from the formation of a He-divacancy complex suggests that, if the temperature needed to induce divacancy diffusion is reached, they seek out and trap He interstitials. The trapping itself involves no activation energy[19] and it occurs by divacancy migration during ion implantation itself. This mechanism suggests that the bubbles formation efficiency is limited by the number of divacancies present in the sample and that it can be improved if a larger amount of vacancies is available during or immediately after the He implant. The second implant creates an additional flux of vacancies that can induce further and deeper bubble formation in the presence of a still substantial helium concentration. The vacancy trapping is then only limited by the He concentration. This effect has been recently noticed in double He^+ and H^+ implants used to obtain the exfoliation of Si layers in SOI (silicon on insulator) application. He^+ and H^+ coimplantation results in a reduction of the total ion implantation dose necessary for exfoliation.[26,27]

The presence of helium inside the bubbles has been deduced by photoluminescence measurements. As-implanted samples do not give any well-defined peak due to the high level of damage, but just a broad peak around 1324 nm. After an annealing at 250 °C for 1 h several peaks appear as shown in the spectrum of Fig. 3(a). In the same figure a photoluminescence signal of a Si self-implanted sample is reported for comparison. The peak at 1216 nm is due to divacancies. Helium inside divacancies perturbs only slightly the reconstructed defect according to molecular dynamics calculations and a strain-based model.[28,29] No change in the electronic configuration occurs, but the reconstructed bonds are just weakened. So, only a slight shift of the main peak is expected. The PL spectra reported in Fig. 3(a) show two very close peaks at 1216 and 1225 nm, respectively. We may attribute them to divacancies and to divacancies filled with helium atoms, respectively. We observed the double peak in samples implanted below and above the critical dose to observe bubbles directly by TEM.

The broad peak, around 1324 nm, was not detected in self-implanted Si samples, or samples implanted below the critical dose. The only structural difference observed by TEM analyses in the samples is the presence of the bubbles. So we can relate this broad peak as signal of vacancy clusters filled with helium (bubbles). The wide peak is due to the large variety of cluster sizes present in the sample. The double peak disappears at temperatures higher than 300 °C,

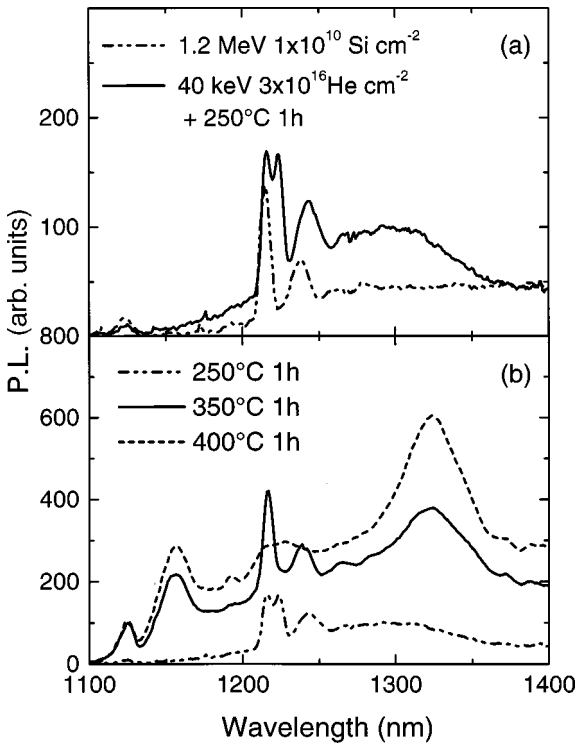

FIG. 3. Comparison between photoluminescence spectra for helium and Si as-implanted samples (a). Photoluminescence spectra of the He implanted samples annealed at different temperatures for 1 h (b).

and a single peak is observed at 1216 nm, i.e., at the divacancy signal, as for example after 350 °C-1 h annealing [see Fig. 3(b)]. The broad peak at 1324 nm increases in amplitude and it is better defined. At 400 °C, also the peak associated with divacancies disappears, while the peak at 1324 nm now is well defined and narrow [Fig. 3(b)]. In summary at temperature lower than the annihilation of divacancies, divacancies filled with He evolve in more complex He-V clusters.

It is well known that divacancies, in ion implanted silicon, disappear at temperature higher than 350 °C.[33] During thermal processes vacancies recombine with silicon self-interstitials emitted by interstitials clusters. A supersaturation of interstitials is surviving, being the balance between vacancies and interstitials in favor of the latter when implanting substitutional species in silicon. Indeed, extra atoms are introduced in the crystal during ion implantation so that the annihilation of vacancies with interstitials produce the vacancy dissolution and the formation of interstitial type residual damage.

This has not been observed when helium is implanted in silicon. Indeed, vacancy type defects are observed even after very high temperature treatments. Apparently, the presence of helium inside divacancy stabilizes them in energy and a different evolution is observed. Probably, by a mechanism similar to that operating in metals,[30] divacancies evolve into more complex He-V clusters (bubbles) while at the same time self-interstitials recombine elsewhere.

Si self-interstitials diffuse very fast even at room temperature so they can be trapped both in the radiation damage close to bubbles, as observed in TEM analyses around the projected range, or at the silicon surface. To determine if Si atoms accumulate at the surface, we prepared ''striped'' implanted samples and we measured the step heights on as-implanted and unimplanted regions as a function of the strip width for several doses. The results are reported in Fig. 4. The step height increases with the width, and a saturation value is reached for values above 3.0 μm. At a width shorter than 3 μm we have to consider in more details the influence of a finite source of defects in the final profile. Indeed, the diffusion of point defects (e.g., interstitials) is isotropic and it can be modeled as one-dimensional only when the affected vertical dimension is quite negligible in comparison with the lateral extension of the source. In this case, the lateral diffusion below the mask region does not contribute significantly to lowering the peak concentration, so that the diffusion of defects can be described in terms of an infinite source. Moreover, the saturation step height increases linearly with the implanted dose suggesting that the phenomenon is directly related to helium implants and to bubble formation. For an implanted dose lower than the critical dose required forming bubbles already visible in TEM analyses no step could be detected by AFM measurements.

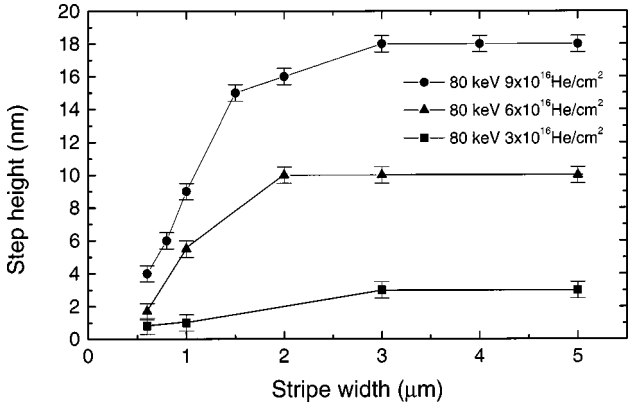

FIG. 4. Step height of helium implanted stripes as a function of the stripe width.

In Fig. 5 the saturation step height value is plotted as a function of the annealing temperature for several doses. The step height remains constant up to 800 °C for the higher implanted doses ($\geqslant 6\times 10^{16}\,\mathrm{cm}^{-2}$) and then decreases. However, at 800 °C almost all the He atoms already left Si and voids are formed, as easily seen in TEM pictures.

In Table I the silicon atoms contained in the step height

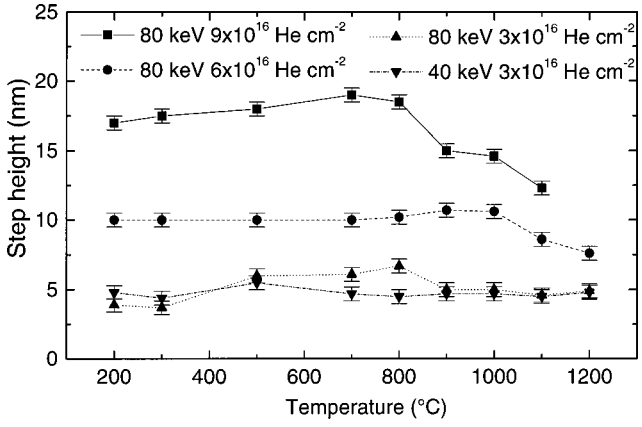

FIG. 5. Saturated step height of helium implanted stripes as a function of annealing temperature.

TABLE I. Si atoms in the step volume are compared with vacancies trapped in the He bubbles for several He implanted samples.

Sample	Si atoms in the step volume [cm^{-2}]	Vacancies in the bubbles [cm^{-2}]
80 KeV $9\times10^{16}\,cm^{-2}$	6×10^{16}	1×10^{17}
80 keV $6\times10^{16}\,cm^{-2}$	3×10^{16}	3×10^{16}
80 keV $3\times10^{16}\,cm^{-2}$	1×10^{16}	1×10^{16}
40 keV $3\times10^{16}\,cm^{-2}$	1×10^{16}	1×10^{16}

volume up to 800 °C annealing are compared with the corresponding vacancy volume of the voids as determined by TEM analyses. The comparison suggests a strong correlation between the silicon missed in the bulk and that trapped at the surface. However, a difference is found for the highest implanted dose, and it can be due to strain of the void layer and to a stressed silicon layer.

The step in the implanted region might be caused by the presence of defects in the lattice. To explore this possibility we performed single crystal x-ray diffraction (XRD) on the annealed samples and the measurements indicate that within the sensitivity limit of the technique, no residual stress is present. Indeed, depth resolved double crystal diffraction (XRD) measurements reported in the literature show the presence of strain at the depth where He is located in the as-implanted samples due to their higher sensitivity.[31] However, this strain is relaxed in a few nanometers for a dose lower than $5\times10^{16}\,cm^{-2}$ and it disappears during the subsequent annealing. At higher doses it increases dramatically, it does not relax during annealing and can induce silicon cutting for fluences $<1\times10^{17}\,cm^{-2}$. Our measurements indicate that the silicon atoms displaced by the bubble formation accumulate at the surface. This causes a bulk supersaturation of vacancies, trapped in the bubbles. At the highest dose some strain is detected, but it cannot be quantified, and indeed the missed silicon in the bulk (voids) alone cannot justify the step height.

With increasing the He^+ fluence a different evolution of damage was observed by TEM analyses. In Fig. 6 the TEM cross sections of samples implanted with $6\times10^{16}\,cm^{-2}$ (a) and $9\times10^{16}\,cm^{-2}$ (b) after 1200 °C 20 min annealing are shown. Up to $6\times10^{16}\,cm^{-2}$ only a void layer is observed. At the higher dose several dislocations are also formed particularly in the lateral sides of the void stripe. These defects we believe are responsible of the difference reported in Table I for the highest dose, between the amount of vacancies in the voids and that of silicon atoms in the step.

Si self-interstitials are also trapped in the silicon layer above the void layer. At higher temperatures (>800 °C) the layer is relaxed and extended defects are observed at the step border (see Fig. 6). Self-ion implantation in crystalline silicon produces point defects as vacancies and self-interstitials. Most of the vacancies and displaced atoms (≈90%) recombine during the implant itself. The remaining ones agglomerate in more complex defects as divacancies, vacancies and interstitial clusters. During annealing, divacancies and vacancy clusters dissolve in the bulk recombining with Si self-interstitials released by the clusters. At temperatures higher

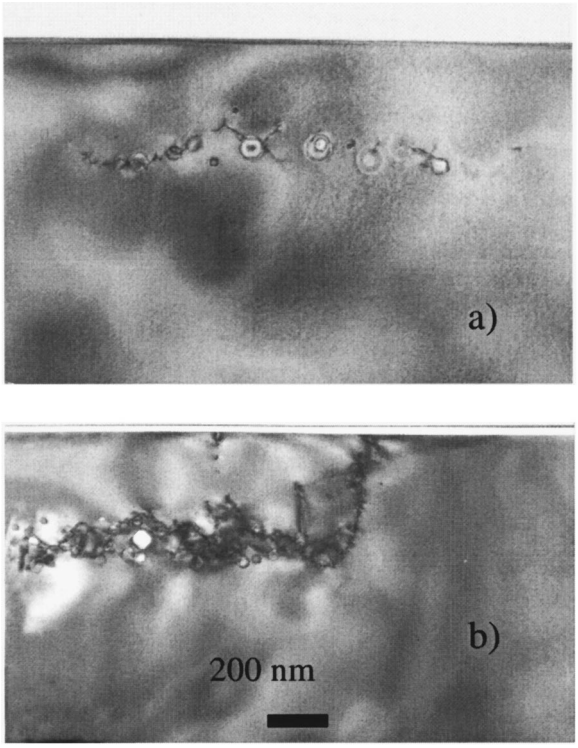

FIG. 6. Cross sections TEM analyses of striped samples implanted with 80 keV $6\times10^{16}\,cm^{-2}$ (a) and $9\times10^{16}\,cm^{-2}$ (b).

than 300 °C, only interstitial type defects are observed. Some interstitial clusters remain at even higher temperatures enlarging in dimensions and forming {311} defects at temperatures around 800 °C. At higher temperatures, these defects generate an interstitial flux and collapse in extended defects.[32] The same trend has been observed for all the implants of impurities that occupy equilibrium substitutional lattice sites. In summary, ion implantation and annealing produces a supersaturation of interstitials in the silicon bulk. After high temperature annealings, interstitials in excess of vacancy concentration, are accommodated in extended defects formed in the bulk. This situation is illustrated schematically in Fig. 7(a) for a low dose helium implantation in silicon, i.e., in the case where bubbles are not formed. The number of defects *per* ion was determined by considering 10% of the displaced silicon atoms calculated by SRIM, which does not consider any recombination.[24] The reported temperature behavior is assumed analogously to similar cases.[33,34] The remaining number of interstitials after 400 °C annealing was determined by TEM analyses on annealed samples.

In the case of high dose helium implants, i.e., when bubbles are formed, a supersaturation of vacancies is created as reported in Fig. 7(b). The vacancies are included in clusters eventually filled with helium atoms (bubbles). Their density and dimension was determined by TEM analysis calculating the number of vacancies/ion. This number increases with the dose. Interstitial type defects have been observed at temperatures up to 800 °C. For annealing temperatures around 800 °C and for a short time, also {311} defects have been observed.[35] However, {311} defects do not collapse in extended interstitial type defects. Indeed, the void formation involves dissolution of interstitial type secondary defects.[36]

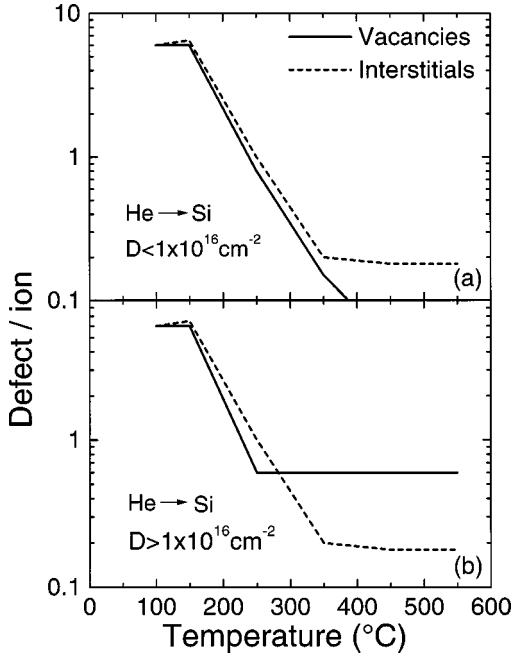

FIG. 7. Vacancies and interstitials related to a single implanted helium ion and determined below (a) and above (b) the dose threshold for bubble formation, as a function of temperature.

As an example TEM cross sections of samples implanted with 100 keV $1\times10^{16}\,\mathrm{cm}^{-2}$ and with 40 keV $3\times10^{16}\,\mathrm{cm}^{-2}$ after a high temperature annealing are reported in Fig. 8. At the threshold dose for bubble formation ($1\times10^{16}\,\mathrm{cm}^{-2}$), both extended defects and voids are observed. Above threshold only voids are observed. In the first case the vacancy-interstitial balance is not yet clearly behalf of vacancies and a hybrid situation is observed. When vacancies superimpose interstitials concentration no interstitial type defects is anywhere observed.

IV. VOID FORMATION AND STABILITY

We have seen that He implants induce heterogeneous nucleation of V clusters. They take place by the interaction of He with divacancies and by the subsequent evolution in more complex He-V agglomerates. This nucleation phase can be described in details only by an atomistic model in molecular dynamic calculations. However, due to the large number of atoms involved a so detailed description has not been so far achieved. The classical nucleation theory[37] is sufficient at this point to describe the formation of voids in silicon.

Assuming a void to be a sphere of radius R_v, in forming it, the crystal free energy is increased by $4\pi R_v^2\sigma$, where σ is the Si surface energy. The number of V trapped in a void is $4\pi R_v^3/(3\Omega)$. At the V concentration per unit volume C_v, the chemical potential of a vacancy is $K_BT\ln(C_v/C_v^{eq})$, where K_B is the Boltzmann's constant, T is the absolute temperature, and C_v^{eq} is the V thermal equilibrium concentration. Hence, the change in the crystal free energy due to V consumption can be written as

$$\left(\frac{4\pi R_v^3}{3\Omega}\right)K_BT\ln\left(\frac{C_v}{C_v^{eq}}\right). \tag{1}$$

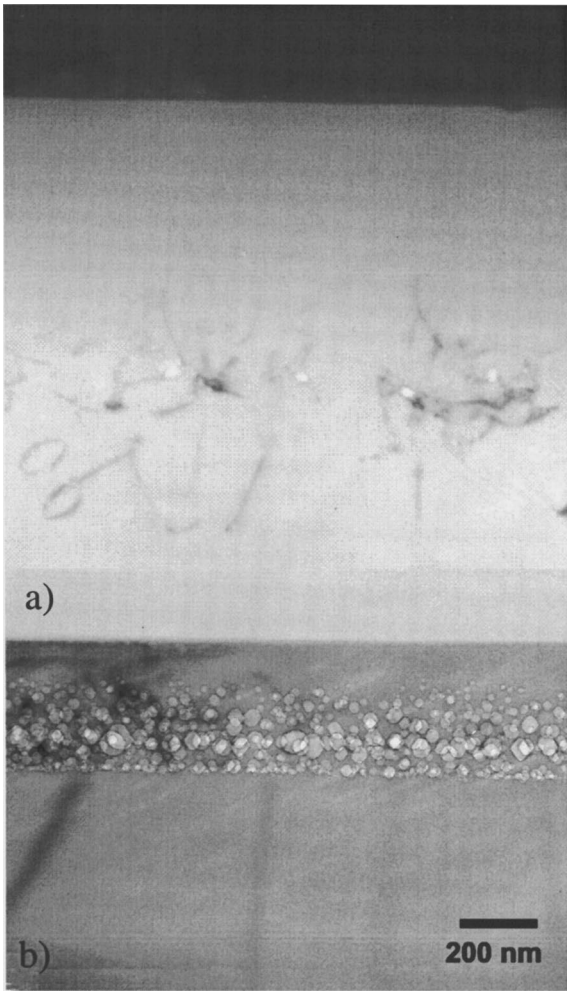

FIG. 8. TEM cross sections of a sample implanted with 100 keV $1\times10^{16}\,\mathrm{cm}^{-2}$ (a) and with 40 keV $3\times10^{16}\,\mathrm{cm}^{-2}$ (b) after high temperature annealing (1000 °C 1 h).

Thus, the net Si crystal free energy change is

$$\Delta G_v = 4\pi R_v^2\sigma - \frac{4\pi R_v^3}{3\Omega}K_BT\ln\left(\frac{C_v}{C_v^{eq}}\right). \tag{2}$$

This energy is zero for $R_v=0$, rises to a maximum value ΔG_v^* at the critical size $R_v=R_v^*$ and then decreases. At the energy maximum the condition

$$\frac{d(\Delta G_v)}{dR_v}=0 \tag{3}$$

yields

$$R_v^* = \frac{2\sigma\Omega}{K_BT\ln\left(\frac{C_v}{C_v^{eq}}\right)}. \tag{4}$$

The V concentration, C_v is obtained by considering 0.6*Φ, i.e., the factor determined from the experimental values (see Fig. 7) multiplied for the He implanted fluence Φ. The V thermal equilibrium concentration C_v^{eq} is given by

$$C_v^{eq} = N\times e^{-E_v/K_BT}, \tag{5}$$

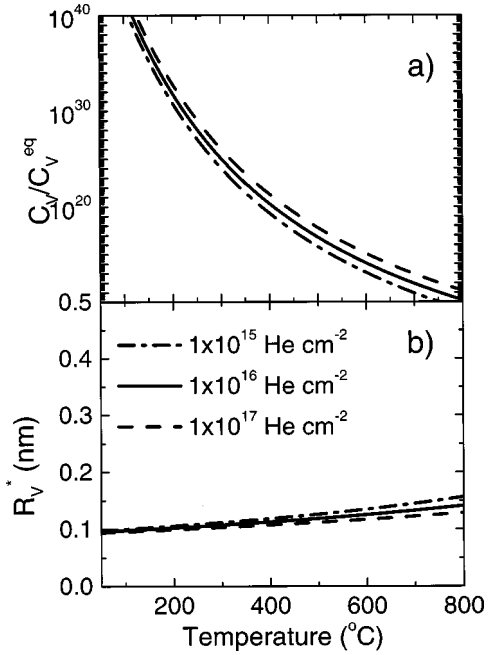

FIG. 9. C_v/C_v^{eq} (a) and R_v^* (b) versus the annealing temperature calculated as described in the text.

where N is the density of silicon, $N=5\times10^{22}$ at/cm^3.

In Fig. 9(a) the C_v/C_v^{eq} ratio versus temperature is drawn for several fluences covering the entirely adopted implant range. The values used for the calculations are $Ev=3.65$ eV,[38] $\Omega=2\times10^{-23}$ cm^3, $\sigma=1230$ ergs cm^{-2}. The R_v^* values versus temperature are reported in Fig. 9(b) for the same implanted doses. The critical radius at the implantation temperature is of the order of 0.1 nm. Indeed, V-He clusters are present in the He as-implanted silicon also at doses below the threshold to form voids after annealing.[31,39] During thermal treatments He desorption occurs and V clusters are left in Si.[25] The V clusters transform into voids only if their dimension overcome the critical radius R_v^*, otherwise they dissolve. However, the calculated critical radius value is too small, so that in principle all clusters should grow. This is not observed experimentally. The reason, as explained in details in the following, is in the role of He in the He-V clusters.

In Fig. 10 the He retained in the sample is reported as a function of the annealing temperature for two different doses, one below and the other above the critical dose for void formation. Below the critical dose (1×10^{16} cm^{-2}) He desorption is observed at a temperature up to 300 °C. In this case the most of He atoms are trapped with divacancies, as observed by photoluminescence, but, due to the low He concentration, they cannot evolve in more complex He-V clusters. So, when helium desorption occurs, divacancies are left in silicon. They evolve as it is well known, and already described.

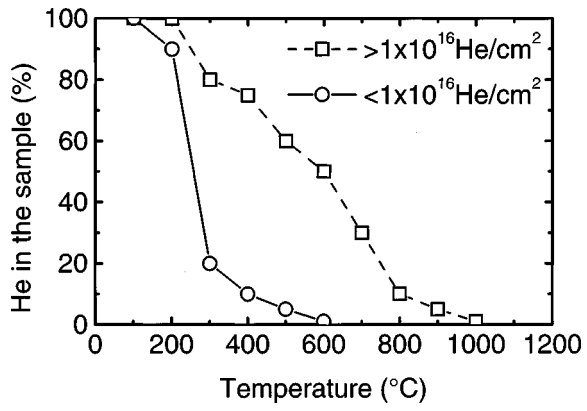

FIG. 10. Measured He in the sample as a function of the annealing temperature.

When bubbles (He-V clusters observed in TEM) are present in the sample the He desorption is retarded (up to 800 °C) so that large vacancies clusters are left after He desorption and moreover at temperatures when interstitials are already arranged in energetically stable configurations. Indeed, we could never observe voids if we could not be able to observe He bubbles in the as-implanted samples by TEM analyses (resolution better than 1 nm).

During annealing at temperatures higher than 300 °C, helium permeates from bubbles above 700 °C desorbs from the sample. In Fig. 11, the p-BS analyses of a double implanted sample with 100 keV 1×10^{17} cm^{-2} and with 40 keV 3×10^{16} cm^{-2} is reported for as-implanted samples (a) and after annealing at 1000 °C, 5 min. (b). Without annealing, the same amount of implanted helium was also measured in the sample. After an annealing at 1000 °C, 60% of the helium left the silicon as we could obtain by the decrease of the He peak area in p-BS analyses. A few percent of the helium remains also after longer annealing. This residual amount of helium cannot justify by itself the stability of voids. Indeed, the voids are unlikely to transform in other defects. The reason can be deduced by comparing the calculated energy for several vacancy type defects.

When a void is formed equilibrium is reached so that the vacancies trapped in the voids do not participate to the concentration of vacancies in the Si crystal. From Eq. (2) we can obtain

$$\Delta G_V=4\pi R_V^2\sigma. \tag{6}$$

The other likely vacancy type defects are dislocation loops. The energy of a loop of radius Rd that may or may not contain also an intrinsic stacking fault (SF) is given by $\pi Rd2\gamma+2\pi Rd(\Gamma/L)$, where γ is the intrinsic SF energy density, Γ/L is the edge dislocation elastic and core energy per unit length[40]

$$\frac{\Gamma}{L}=\frac{\mu b^2}{4\pi(1-\nu)}\left(\ln\frac{8\alpha R_d}{b}-1\right). \tag{7}$$

Here μ is the shear modulus of Si, b is the magnitude of the dislocation Burgers vector, taken to be perpendicular to the loop plane, ν the Poisson' ratio, and α is a dimensionless parameter.

Thus, formation of a dislocation loop causes an increase of the crystal free energy. On the other hand, a certain number of vacancies is consumed which results in a decrease of the crystal free energy. The number of V consumed in forming the loop is $\pi R_d 2b/\Omega$, where Ω is the volume of one V. At the V concentration per unit volume, C_v the chemical poten-

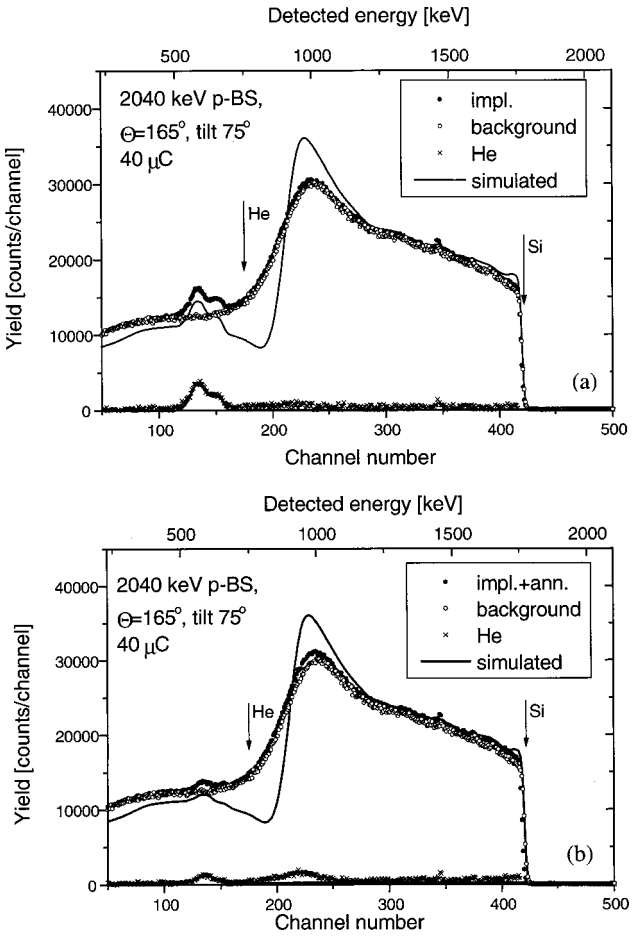

FIG. 11. p-BS spectra of samples implanted with 100 keV $1\times10^{17}\,\mathrm{cm}^{-2}$ and 40 keV $3\times10^{16}\,\mathrm{cm}^{-2}$ obtained for the as-implanted sample (a) and after annealing at 1000 °C for 5 min (b). For comparison a not-implanted (background) and the simulated spectra are shown. The surface position of Si and He are indicated by arrows.

tial of a vacancy is $K_BT\ln(C_\mathrm{v}/C_\mathrm{v}^{\mathrm{eq}})$. Hence, the crystal free energy is decreased by $(\pi R_d 2b/\Omega)K_BT\ln(C_\mathrm{v}/C_\mathrm{v}^{\mathrm{eq}})$. This is valid only if C_v does not change significantly due to its consumption of vacancies to form dislocations, i.e., for $\rho_d\pi R_d 2b/\Omega \ll C_\mathrm{v}$ holding, where ρ_d is the volume density of dislocation loops. This condition is satisfied at the stage of nucleation and therefore can be used to determine the nucleation energy barrier. The net Si crystal free energy change due to nucleation of a dislocation loop is

$$\Delta G_d=\pi R_d^2\gamma+R_d\frac{\mu b^2}{2(1-\nu)}\left(\ln\frac{8\alpha R_d}{b}-1\right)-\frac{\pi R_d^2 b}{\Omega}K_BT\ln\frac{C_\mathrm{v}}{C_\mathrm{v}^{\mathrm{eq}}}. \tag{8}$$

The energy of the defects are defined by Eqs. (2) and (8) by considering the equilibrium condition $C_\mathrm{v}=C_\mathrm{v}^{\mathrm{eq}}$. We have calculated the defect energy by using the parameters: $\Omega=2\times10^{-23}\,\mathrm{cm}^3$, $\sigma=1230\,\mathrm{ergs\,cm}^{-2}$, $\gamma=60\,\mathrm{ergs\,cm}^{-2}$ for the faulted dislocation loop and 0 ergs cm^{-2} for the perfect dislocation loop, $\mu=6.45\times10^{11}\,\mathrm{dyne\,cm}^{-2}$, $\nu=0.228$, $\alpha=4$, $b=3.135\times10^{-8}$ cm for the $\langle111\rangle/3$ Frank partial dislocation loop and 3.84×10^{-8} cm for the $\langle110\rangle/2$ perfect loop. The results are reported in Fig. 12. Voids containing less that 4×10^7 vacancies (≈50 nm in diameter) are the most stable defect. Even after very high temperature annealing for long time (1200 °C for 5 h) the larger void was less than 50 nm, i.e., it is unlikely that when formed, even after helium desorption, voids collapse in different defect type.

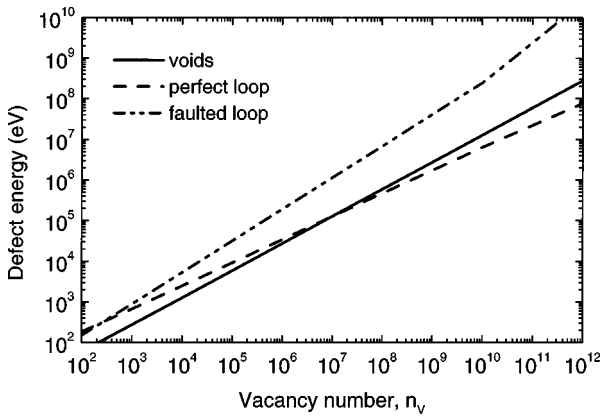

FIG. 12. Defect energy for a void, a perfect loop, and a faulted loop versus the vacancy number.

V. CONCLUSION

An enlargement of a bubble layer formed by high dose He implantation has been systematically observed when a second implant is performed. This is due to He vacancies interaction. Helium is repelled by vacancies and forced to an enhanced diffusion during implantation. Helium atoms are instead trapped by divacancies stabilizing them and favoring their evolution into more complex He-V clusters at temperature up to 400 °C. The displaced silicon atoms, produced during implantation, recombine at the surface in the same range of temperatures. The result is a supersaturation of vacancies in the silicon bulk, contrary to the ordinary ion implantation and annealing. This vacancy supersaturation is also responsible of the secondary defect suppression.

Clusters of vacancies evolve in bubbles only if their dimension overcomes the critical radius. Voids with a few percent of originally implanted helium atoms remain also after He desorption. This is because the void is a stable defect and its energy is the lower respect other defect accommodation of vacancies. The vacancy supersaturation in voids is observed even after thermal treatment at 1200 °C for 5 h.

ACKNOWLEDGMENTS

We wish to acknowledge Professor S. U. Campisano for his contribution to our work. The authors acknowledge MADESS II for financial support, the CNR-Hung. Acad. Sci. scientific cooperation for travel funds, and the partial financial support of OTKA Grant Foundation (Hungary), Contract Nos. T 025928 and F019165. The technical assistance of M. Furnari has been appreciated during AFM analyses.

[1] R. Blackburn, Metall. Rev. **11**, 159 (1966).
[2] S. E. Donnelly, Radiat. Eff. **90**, 1 (1985).
[3] D. J. Reed, Radiat. Eff. **31**, 129 (1977).
[4] R. G. Elliman, S. T. Johnson, K. T. Short, and J. S. Williams, in *Ion Implantation and Ion Beam Processing of Materials*, edited by G. K. Hubler, O. W. Holland, C. R. Clayton, and C. W. White, MRS Symposia Proceedings No. 27 (Materials Research Society, Pittsburgh, 1984), p. 229.
[5] S. M. Myers, H. J. Stein, and D. M. Follstaedt, Phys. Rev. B **51**, 9742 (1995).
[6] S. K. Das and M. Kaminsky, Adv. Chem. Ser. **158**, 112 (1976).
[7] F. Pászti, G. Mezey, L. Pogány, M. Fried, A. Manuaba, E. Kótai, T. Lohner, and L. Pócs, Nucl. Instrum. Methods Phys. Res. **209/210**, 1001 (1983).
[8] F. Pászti, A. Manuaba, L. Pogány, G. Vízkelethy, M. Fried, E. Kótai, H. V. Suu, T. Lohner, L. Pócs, and G. Mezey, J. Nucl. Mater. **119**, 26 (1983).
[9] S. M. Myers, G. A. Petersen, and C. H. Seager, J. Appl. Phys. **80**, 3717 (1996), and reference therein.
[10] V. Raineri, Solid State Phenom. **57–58**, 43 (1997), and reference therein.
[11] V. Raineri and S. U. Campisano, Nucl. Instrum. Methods Phys. Res. B **120**, 56 (1996).
[12] C. H. Seager, S. M. Myers, R. A. Anderson, W. L. Warren, and D. M. Follstaedt, Phys. Rev. B **50**, 2458 (1994).
[13] V. Raineri, P. G. Fallica, G. Percolla, A. Battaglia, M. Barbagallo, and S. U. Campisano, J. Appl. Phys. **78**, 3727 (1995).
[14] M. Saggio, V. Raineri, R. Letor, and F. Frisina, IEEE Electron Device Lett. **18**, 333 (1997).
[15] N. Q. Khánh, P. Tüttõ, E. N. Jároli, O. Buiu, L. P. Bíró, F. Pászti, T. Mohácsi, C. Kovacsics, A. Manuaba, and J. Gyulai, Mater. Sci. Forum **248–249**, 101 (1997).
[16] V. Raineri and M. Saggio, Appl. Phys. Lett. **71**, 1673 (1997).
[17] V. Raineri, S. Coffa, M. Saggio, F. Frisina, and E. Rimini, Nucl. Instrum. Methods Phys. Res. B **147**, 292 (1999).
[18] M. Alatalo, M. J. Puska, and R. M. Nieminen, Phys. Rev. B **46**, 12 806 (1992).
[19] S. K. Estreicher, J. Weber, A. Derecskei-Kovacs, and D. S. Marynick, Phys. Rev. B **55**, 5037 (1997).
[20] F. Pászti, Nucl. Instrum. Methods Phys. Res. B **66**, 83 (1992).
[21] F. Pászti, A. Manuaba, E. Szilágyi, and Z. Vértessy, Nucl. Instrum. Methods Phys. Res. B **117**, 253 (1996).
[22] F. Pászti, A. Manuaba, C. Hajdu, A. A. Melo, and M. F. da Silva, Nucl. Instrum. Methods Phys. Res. B **47**, 187 (1990).
[23] E. Kótai, Nucl. Instrum. Methods Phys. Res. B **85**, 588 (1994).
[24] J. F. Ziegler, J. P. Biersack, and U. Littmark, *The Stopping and Range of Ions in Solids* (Pergamon, New York, 1985).
[25] F. Corni, C. Nobili, G. Ottaviani, R. Tonini, and G. Calzolari, Phys. Rev. B **56**, 7331 (1997).
[26] A. Agarwal, T. E. Haynes, V. C. Venezia, O. W. Holland, and D. J. Englesham, Appl. Phys. Lett. **72**, 1086 (1998).
[27] M. K. Weldon, M. Collot, Y. J. Chabal, V. C. Venezia, A. Agarwal, T. E. Haynes, D. J. Eaglesham, S. B. Christman, and E. E. Chaban, Appl. Phys. Lett. **73**, 3721 (1998).
[28] G. Davies, Phys. Rep. **176**, 83 (1989).
[29] G. Davies, E. C. Lightowlers, and Z. F. Ciedanawaska, J. Phys. C **20**, 191 (1987).
[30] D. J. Reed, Radiat. Eff. **31**, 129 (1977).
[31] F. Corni, G. Calzolari, S. Frabboni, C. Nobili, G. Ottaviani, R. Tonini, G. F. Cerofolini, D. Leone, M. Servidori, R. S. Brusa, G. P. Karwasz, N. Tiengo, and A. Zecca, J. Appl. Phys. **85**, 1401 (1999).
[32] J. L. Benton, S. Libertino, P. Kringoi, D. J. Eaglesham, J M. Poate, and S. Coffa, J. Appl. Phys. **82**, 120 (1997).
[33] S. Libertino, J. L. Benton, D. C. Jacobson, D. J. Eaglesham, J. M. Poate, S. Coffa, P. G. Fuochi, and M. Lavalle, Appl. Phys. Lett. **71**, 389 (1997); S. Libertino, S. Coffa, J. L. Benton, K. Halliburton, and D. J. Eaglesham, Nucl. Instrum. Methods Phys. Res. B **148**, 247 (1999).
[34] S. Libertino, S. Coffa, J. L. Benton, K. Halliburton, and D. J. Eaglesham, Nucl. Instrum. Methods Phys. Res. B **148**, 247 (1999).
[35] F. Roqueta, A. Grob, J. J. Grob, R. Jerisian, J. P. Stoquert, and L. Ventura, Nucl. Instrum. Methods Phys. Res. B **147**, 298 (1999).
[36] V. Raineri and S. U. Campisano, Appl. Phys. Lett. **69**, 1783 (1996).
[37] J. W. Christion, *The Theory of Transformation in Metals and Alloys*, 1st ed. (Pergamon Press, NY, 1965), Chap. X.
[38] M. Tang, L. Colombo, J. Zhu, and T. Diaz de la Rubia, Phys. Rev. B **55**, 14 279 (1997).
[39] R. S. Brusa, G. P. Karwasz, N. Tiengo, A. Zecca, F. Corni, G. Calzolari, and C. Nobili, J. Appl. Phys. **85**, 2390 (1999).
[40] J. P. Hirth and J. Lothe, *Theory of Dislocations* (McGraw-Hill, New York, 1968), p. 145.